Chemical Oxidation of Graphite: Evolution of the Structure and Properties

Viera Skákalová[1,2,], [3]Peter Kotrusz[1], Matej Jergel[4], Toma Susi[2], Andreas Mittelberger[2], Viliam Vretenár[1,5], Peter Šiffalovič[4], Jani Kotakoski[2], Jannik C. Meyer[2] and Martin Hulman[1,3]*

[1]Danubia NanoTech, Ilkovičova 3, 84104 Bratislava, Slovakia

[2]University of Vienna, Boltzmanngasse 5, 1090 Vienna, Austria

[3]Institute of Electrical Engineering SAS, Dúbravská cesta 9, 84104 Bratislava, Slovakia

[4]Institute of Physics SAS, Dúbravská cesta 9, 84104 Bratislava, Slovakia

[5]Center for Nanodiagnostics of SUT, Vazovova 5, 81000 Bratislava, Slovakia

ABSTRACT

Graphene oxide is a complex material whose synthesis is still incompletely understood. To study the time evolution of structural and chemical properties of oxidized graphite, samples at different temporal stages of oxidation were selected and characterized through a number of techniques: X-ray photoelectron spectroscopy for the content and bonding of oxygen, X-ray diffraction for the level of intercalation, Raman spectroscopy for detection of structural changes, electrical resistivity measurements for probing charge localization on the macroscopic scale, and scanning

transmission electron microscopy for the atomic structure of the graphene oxide flakes. We found a non-linear behavior of oxygen uptake with time where two concentration plateaus were identified: uptake reached 20 at.% in the first 15 minutes, and after one hour a second uptake started, reaching a highest oxygen concentration of more than 30 at.% after two hours of oxidation. At the same time, the interlayer distance expanded to more than twice the value of graphite and the electrical resistivity increased by 7 orders of magnitude. After four days of chemical processing, the expanded structure of graphite oxide became unstable and spontaneously exfoliated; more than two weeks resulted in a significant decrease of the oxygen content accompanied by re-aggregation of the GO sheets. These correlated measurements allow us to offer a comprehensive view into the complex oxidation process.

INTRODUCTION

Graphene oxide (GO) is a material made of atomically thin graphitic sheets prepared by the oxidation of graphite[1,2]. It is widely considered as a precursor for the large-scale production of graphene upon reduction. On the other hand, GO is a subject of research for many potential applications including supercapacitors[3-6], solar cells[7-9], memory devices[10] and bio-inspired systems[11-15]. There are several chemical routes to GO[16-18], all based on the use of strong oxidizing agents (OA). One of the properties sensitively reflecting the structural disorder in graphene is charge transport. As a consequence of covalent functionalization, charge localization eliminates conductance in GO. Removing the functional groups by chemical or thermal methods to some extent restores charge delocalization[19-26]. To minimize the negative effect of the chemical treatment on the atomic structure it is necessary to understand the relation between the structure, properties and the oxidation process of graphite from the beginning.

A number of reports have been published discussing the kinetics of graphite oxidation and exfoliation by the modified Hummers method. Nevertheless, the reported results vary with differently modified process conditions. A mechanism of GO formation was recently discussed in papers published by the Tour group[27,28]. In their variant of the Hummers method, they observed three steps leading to the formation of GO. In the first, graphite is intercalated by sulfuric groups. In the second step, the intercalated graphite evolves into oxidized graphite while keeping its c-axis order, which, after exposure to water, is eventually completely lost in the final step of GO formation upon exfoliation. However, graphite intercalation by sulfuric acid prior to oxidation is not always observed. An oxidation mechanism involving the transformation of different oxygen groups both at the edges and on the basal planes was proposed in Ref. 29. These processes lead inevitably to a destruction of the aromatic structure in GO[30], and the interlayer separation of graphitic sheets probed by X-ray diffraction (XRD) does not increase after the oxidation reaches a certain level. In Ref. 31, different levels of oxidation were achieved by changing the amount of oxidizing agent while keeping the reaction time constant. The authors observed an oxidation-dependent increase of the interlayer spacing in the XRD experiment, whereas X-ray photoelectron spectroscopy (XPS) suggested the formation of hydroxyl and carbonyl groups and their conversion into epoxide groups as the oxidation progressed. Raman spectra of the oxidized samples were interpreted to show an increasing proportion of sp[3] domains and the disruption of the graphitic stacking order. Similar results were obtained for samples oxidized for various times between 30 minutes and three days[32]. XPS measurements indicated that an oxygen saturation of the graphite framework was reached within two hours. The interlayer separation increased from 0.35 nm to 0.79 nm after 30 minutes of oxidation, and in addition, the graphitic peak at $2\Theta =$

26.6° disappeared completely from the XRD diffractogram. In the following three days of oxidation, the interlayer distance enlarged only slightly up to 0.84 nm.

In this work, we present more extensive experiments on graphite oxidation by a Hummers' method, spanning a time scale from minutes to several weeks. We trace a gradual change of the material properties and characterize the samples with multiple methods along the oxidation process. Our aim was to identify the stage when the conversion of graphite to GO is completed. Going beyond previous reports, we observed a spontaneous exfoliation accompanied by a significant reduction of oxygen content (from ~30 at.% down to ~20 at.%) and a consequent re-aggregation of GO flakes after very long processing times.

EXPERIMENTAL SECTION

Sample preparation

Our graphene oxide synthesis follows a procedure described in Ref. 33. In this modification of the Hummers method, a larger amount of sulfuric acid is used compared to the standard procedure[2]. However, a similar amount of the acid has also been used by others[28].

In brief, graphite powder of microcrystal grade, purity of 99.9995% and size of 2-15 μm was purchased from Alfa Aesar. Sulfuric acid (350 ml) was mixed with graphite (2 g) at 0 °C for 15 min. After that, a small portion of the graphite dispersion in sulfuric acid was taken for characterization, defining time "zero" on our oxidation time scale. Next, potassium permanganate (8 g) and sodium nitrate (1 g) were added portion-wise every 15 min at 0 °C in a total of 11 portions. Just prior to when a next portion of oxidation agents was added, another liquid fraction was taken from the reaction mixture. The reaction was terminated by adding 500 ml of deionized water and 40 ml of 30 % H_2O_2. Each fraction was filtered off through a nylon

filter, washed with diluted (10%) HCl to remove metal ions, and then with water until the pH of the filtrate was close to 7, and finally dried at 75 ᵒC. After the last dose of the oxidizing agent was added at 150 min, the reaction mixture was then stirred for 30 min at 0 ᵒC and for further 30 min at 35 ᵒC. After that, water (250 ml) was added via a dropping funnel and the reaction mixture was heated up to 98 ᵒC and held at that temperature for up to 5 weeks. Other fractions were regularly (after days and weeks) taken from the mixture for analysis.

For scanning transmission electron microscopy (STEM) imaging, TEM-grids were dipped into fractions of GO suspended in water. For electrical resistivity measurements, fractions were filtrated through polypropylene filters with 0.4 μm pore size to obtain freestanding membranes.

Sample characterization

XPS measurements were carried out using a high-performance spectrometer (Thermo Fischer) with monochromatized Al $K\alpha$ radiation (1486.6 eV). C $1s$ peaks were fitted by a combination of Gaussian and Lorentzian line shapes.

Raman spectroscopy was performed with a scanning confocal setup N-TEGRA, where the laser beam of a solid state laser with a wavelength of 472 nm and a power of 4 mW was circularly polarized and focused to a diffraction-limited spot approximately 400 nm in size. At each position, the backscattered light was dispersed in a monochromator and detected with a Peltier-cooled charge coupled device (CCD) with an accumulation time of 1 s.

XRD was measured by a D8 DISCOVER SSS diffractometer (Bruker AXS) equipped with 18 kW Cu rotating anode generator in the parallel-beam grazing-incidence geometry at an angle of incidence of 1°. To get a planar sample for the measurement, the GO powder was applied onto a

microscopy glass plate covered with a small amount of vaseline and pressed briefly by another glass. The small angle of incidence eliminated the effect of support on the diffraction pattern.

Electrical resistivity was measured in four-probe configuration using parallel gold strips evaporated onto the surface of thin GO films as electrodes. A constant current of 100 nA applied to the outer electrode pair was supplied by a source-meter Keithley 2635B while resistance was evaluated between the central electrode pair (electrode configuration is presented in Fig. S1). Temperature during the measurement was probed by a Si-diode thermometer.

STEM experiments were conducted using a Nion Ultra-STEM100 scanning transmission electron microscope, operated at 60 kV in near-ultrahigh vacuum ($2x10^{-7}$ Pa). The beam current during the experiments was a few tens of pA, corresponding to a dose rate of approximately $1x10^{7}$ e^{-}/Å^{2}s. The beam convergence semi angle was 35 mrad and the semi-angular range of the medium-angle annular dark field (MAADF) detector was 60–80 mrad.

Density functional theory (DFT) simulations were conducted using the GPAW software package[34], with van der Waals interactions included via an appropriate exchange-correlation functional[35]. Equilibrium distances of functionalized bilayer graphene were found by relaxing the structure of a 4×4 supercell with 20 Å vacuum in the perpendicular direction using a 0.19 Å grid spacing and a 5×5×1 k-point mesh until maximum forces were <0.01 eV/Å, and measuring the separation of facing C atoms away from the functional site.
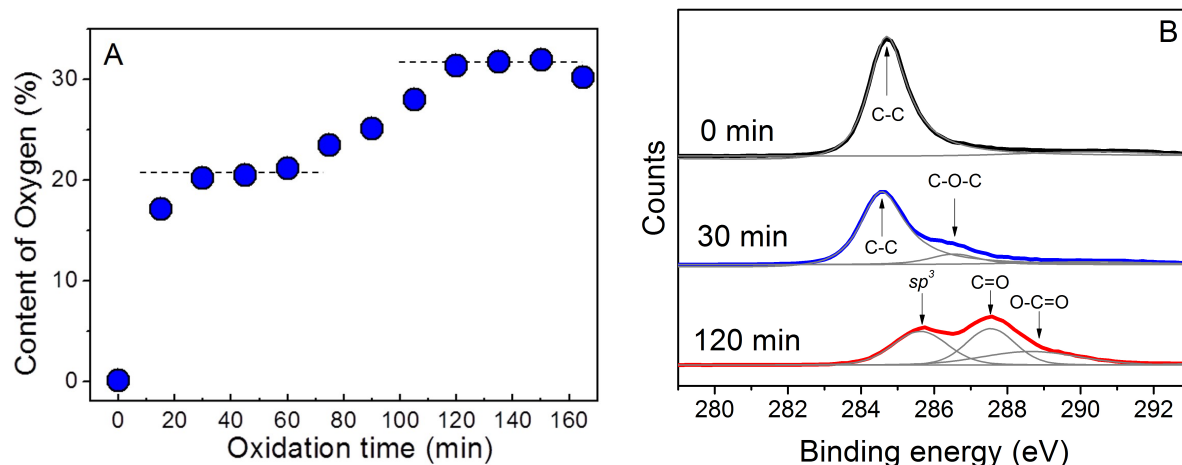
RESULTS AND DISCUSSION

Figure 1. (A) Content of oxygen in graphite versus oxidation time detected by XPS, (B) characteristic XPS spectra of fractions from the three distinct regimes observed in (A): at time "0 min" before introducing the OA (black), after 30 min when reaching the first plateau (blue) and after 120 min of reaching the second plateau (red).

The progression of graphite oxidation is illustrated in Figure 1A, where we plot the content of oxygen measured by XPS versus time from the beginning of the oxidation process. A rapid uptake of 17 at.% oxygen is observed already 15 minutes after introducing the first dose (10%) of oxidation agents (OA). Then, despite progressive addition of OA, oxygen concentration hardly changes, saturating at around 20 at.%. Only after 75 minutes when 50% of OA was added into the mixture, we observed additional uptake of oxygen. The steady increase continues until 120 minutes (80% of OA) when the oxygen content saturates again at a maximum value of more than 31 at.%. The last dose of OA is added at 150 min.

Figure 1B presents XPS spectra of the carbon C 1*s* level, which demonstrate changes in bonding or the carbon atoms during the oxidation of graphite. Here we choose three representative spectra that are related to the zero-time fraction and to the fractions after 30 and 120 min of oxidation, where two saturation regimes in the uptake of oxygen were observed. The spectrum of graphite treated with sulfuric acid only is assigned to 0 minute (black curve) and shows a single peak at 284.7 eV related to C-C bond in sp[2] hybridization[36,37]. This is consistent with the fact that sulfuric acid neither intercalated nor oxidized graphite within our experimental conditions[38]. Besides the peak at 284.7 eV, a new shoulder centered at ~286.6 eV is formed in the spectrum taken after 30 min oxidation, indicating 13 % of C-O-C bonds is present. The XPS spectrum of the fraction with 80 % of OA processed for 120 min (red curve) shows a dramatic change in chemical nature of carbon-oxygen bonds. Two wide peaks at higher binding energies dominate: the one at 285.6 eV results from sp[3] hybridized C-C bonds and the peak at 287.6 eV corresponds to C=O species. There is also a weak band at 288.6 eV due to O-C=O bonds[39,40, 41]. A summary of carbon chemical bonding related to the amount of OA is provided in Table S1 of the Supplementary Information.
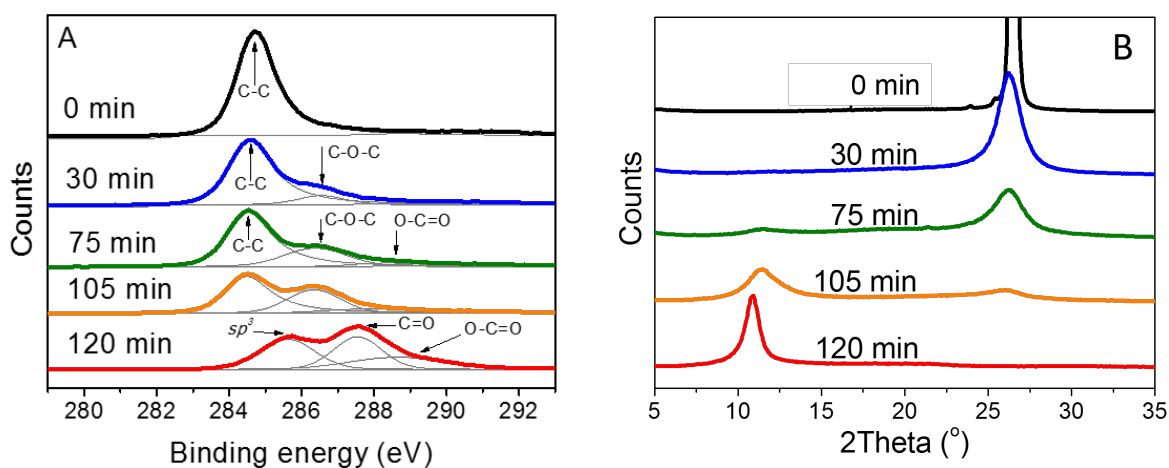

Figure 2. Evolution of the XPS (A) and XRD (B) signal during the oxidation from 0 to 120 min.

The oxidation of graphite causes a significant expansion of the hexagonal crystal lattice in the *c*-axis ([001]) direction. To understand the relations between the oxidation kinetics of graphite and changes in its crystal structure we correlate XPS (Fig. 2A) with the corresponding XRD (Fig. 2B) diffractograms, progressively acquired during the oxidative intercalation. Figure 2A presents the XPS signal development in more detail. The black curve in Figure 2B shows the 0th fraction (graphite treated in sulfuric acid only), exhibiting an intensive and narrow (FWHM = 0.7°) diffraction peak centered at $2\Theta = 26.5°$ due to an interlayer spacing of 0.34 nm in the [001] crystallographic direction, identical to that of graphite. Adding 20% of OA at 30 min causes this peak to decrease, widen and slightly shift to lower angles. In this stage the detected content of oxygen was already more than 20 at.%, mostly in the C-O-C binding state. This amount is too large to be explained by oxygen binding to carbon only on the surfaces and edges of graphitic grains (as a simple estimate, a cubic graphite grain with a volume of 1 μm³ has only 0.04% of carbon atoms on its surface). Oxidizing agents must therefore diffuse between the graphitic layers.

However, we did not find any signatures of graphite intercalated by sulfuric acid at 22.3° in our XRD measurements, contrary to previous observations[28]. We instead observe a very small shift of the peak maximum (-0.5°) and its widening. The increasing background signal and decreasing graphitic peak in the XRD diffractograms of Fig. 2B suggests that the oxidized areas are randomly distributed over the volume of the graphitic grains. The peak completely vanishes after adding 80 % of OA (120 min) when the concentration of oxygen reaches ~31 at.% and the graphitic spacing is lost. A new diffraction peak at 10.9° is formed as a consequence of graphite oxidative intercalation with (mostly) C=O and O-C=O oxide species identified by XPS (bottom spectrum in Fig. 2A). To form a quantitative picture of the different oxygen bonding forms, the

XPS curves are fitted by the smallest number of peaks at this stage when the oxidative intercalation is complete. The initial interlayer spacing of graphite expanded more than twofold up to 0.81 nm in graphite oxide, and the long-range order in the *c*-axis direction is restored. We also observed that the interlayer spacing depends on both the size of a starting graphitic powder and the temperature at which the GO dispersion was finally dried. In particular, the latter dependence is quite strong and the interlayer spacing may vary within about 0.1 nm depending on the temperature. The details are shown in the Supporting Information Figs. S2a and S2b.

The XPS and XRD observations clearly indicate two phases during the oxidative intercalation of graphite characterized by these features: (i) until 75 min we see a formation of C-O-C bonded species; the graphitic phase still persists, but a part of the structure becomes oxidatively intercalated. (ii) After ~75 min, a new uptake of oxygen, mostly forming C=O and O-C=O groups, is related to complete oxidative intercalation. After 120 min, a new ordering in the c-axis direction is established.

To help understand the influence of oxidation on the graphite lattice spacing, we turned to density functional theory to calculate the equilibrium distance of bilayer graphene with different oxygen-containing functional groups. The spacing for a pristine bilayer was found to be 3.61 Å, close to the expected graphite interlayer distance. The inclusion of an oxygen functional group on one layer increased the distance to 4.05, 4.65 and 5.69 Å respectively for O, OH and COOH groups. By introducing identical groups on equivalent facing sites we found equilibrium distances of 6.22 and 6.74 Å for double O and OH groups. While being still slightly smaller than the observed spacing in the fully oxidized sample, the steric hindrance of functional groups on two facing graphene oxide lattices has been found to increase the spacing by ~20 % (Ref. 34), thus bringing the simulation into good agreement with the XRD data.
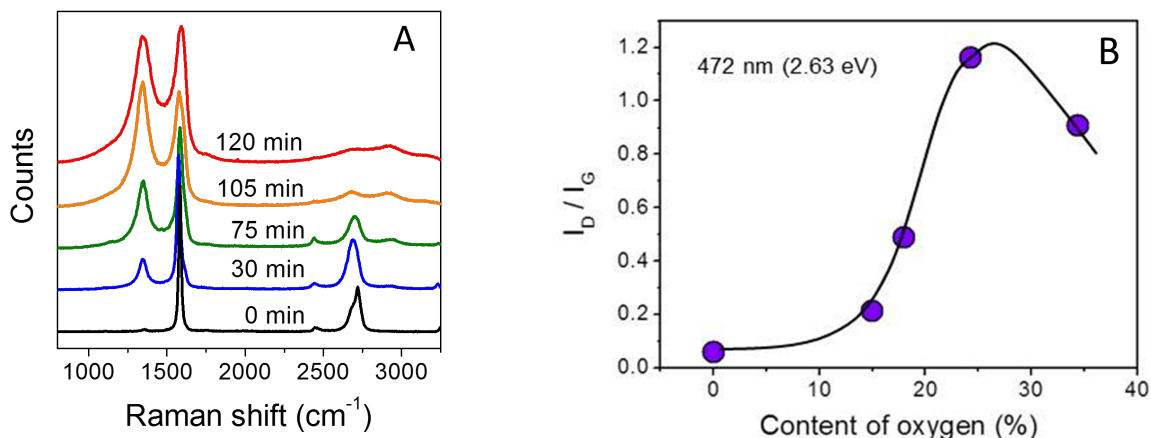
Figure 3. (A) Evolution of Raman spectra during graphite oxidative intercalation, (B) D- to G-mode intensity ratio for different oxygen contents.

The formation of defects during oxidation is reflected in the set of Raman spectra measured with a blue laser excitation of 2.63 eV at particular stages of oxidation (Figure 3A). As the oxidation progresses, the G band at ~1585 cm^{-1} gets broader and the 2D band at ~2680 cm^{-1} gradually disappears, eventually developing a series of broad features between 2600 cm^{-1} and 3000 cm^{-1}. On the other hand, the defect-induced D band increases in intensity overtaking the G mode, but then widens and slightly decreases after the intercalation has been completed. In Figure 3B we plotted the ratio of intensities of the D- to G-modes as a function of the content of oxygen, from which a mean distance between defects can be evaluated[42,43]. In our sample containing about 31 at.% of oxygen, the mean distance is as small as[40] 1.5 nm. This is in a good agreement with the STEM images in Figure 4, which visualize the amorphous atomic structure of GO after 165 min of oxidation. Besides various non-hexagon rings and pores visible in the single layer, there is abundant atomic contamination. Most of the brighter spots in the images in Figure 4 are likely atoms of oxygen and silicon as the presence of these elements have been identified by electron energy loss spectroscopy (EELS; see Fig. S3).
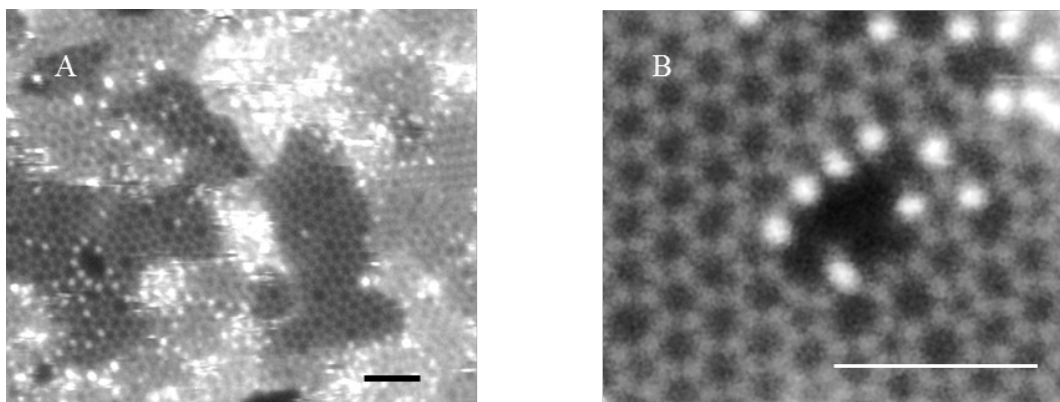
Figure 4. STEM images of a GO layer after 165 min of oxidation at (A) smaller and (B) greater magnification; scale bars correspond to 1 nm.
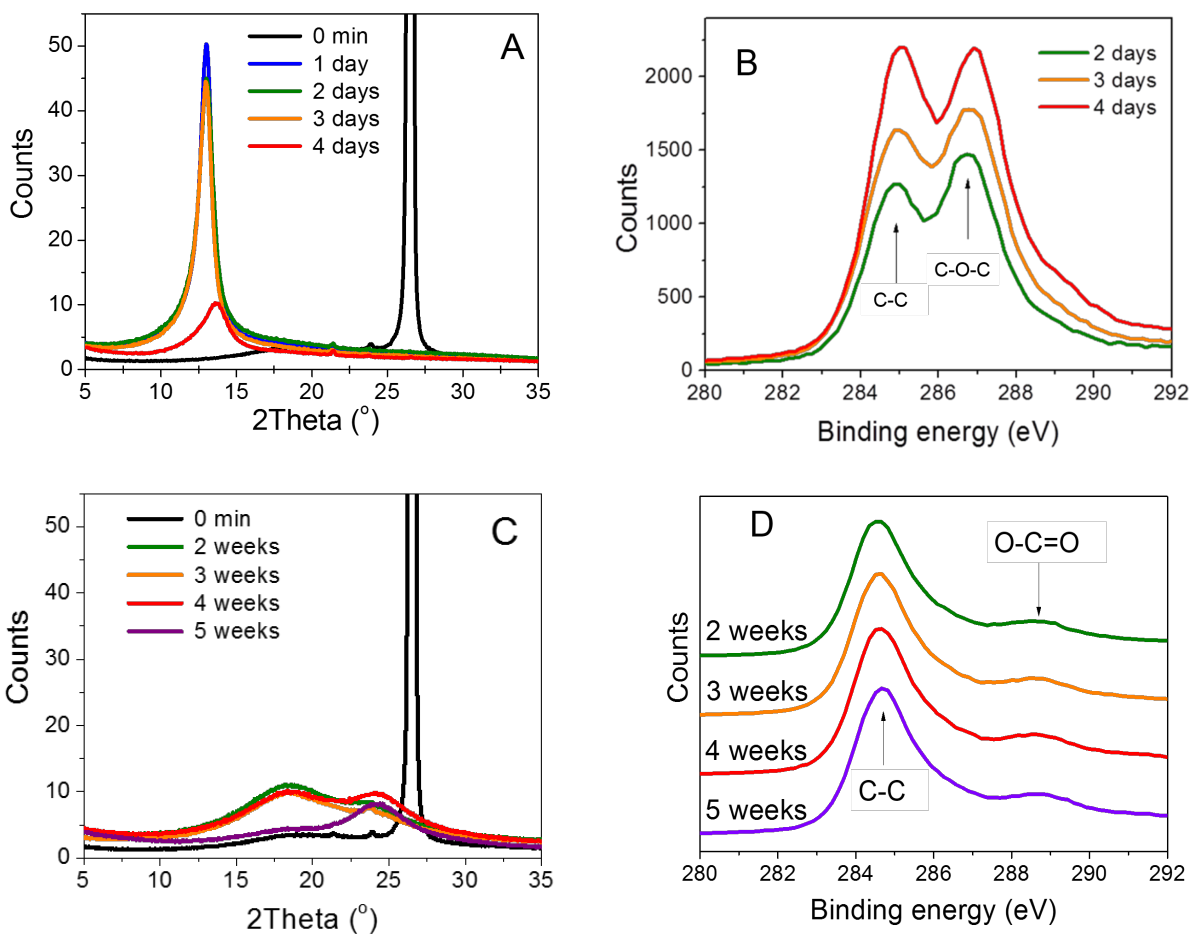

Figure 5. (A) XRD and (B) XPS evolution after days of oxidation, (C) XRD and (D) XPS evolution after weeks of oxidation.

We continued to follow the structural evolution long beyond the point of full graphite intercalation. Interestingly, the XRD results in Figure 5A indicate that 1–3 days of reaction do not lead to a greater expansion of the lattice, but the structure of graphite oxide on the contrary densifies, showing a relatively intensive and narrow diffraction peak centered at 12.6° (layer spacing of 0.70 nm). After 4 days, however, the peak intensity drops and it shifts to higher diffraction angles. Meanwhile, the XPS measurements (Fig. 5B) indicate a decreasing concentration of oxygen in the sample within a time scale of days as the lower energy peak related to C-C binding progressively increases relative to the C-O-C peak at 286.7 eV.

The XRD results of weeks-long oxidized graphite are plotted in Figure 5C. This oxidation led to the apparent exfoliation of intercalated graphite as the sharp peak at 12.6° disappeared; an atomic force microscope image (Figure S4 in Supporting Information) demonstrates mainly single GO layers present after exfoliation. The disordered layers then partially re-aggregate forming finally a ridge close to 24° (Figure 5C). Proximity of this ridge to the graphite peak position suggests a partial recovery of the interlayer spacing. This can be possible only if covalently bonded oxygen is released. Indeed, in the XPS spectra (Figure 5D) we detected a significant decrease of oxygen in the sample after extremely long times of oxidation. Besides this, the XPS spectra do not show significant development between 2 to 5 weeks of oxidation time; in particular, the sp^3/sp^2 ratio is independent of oxidation time[44]. Although we cannot provide direct evidence of the release of CO_2 molecules from our material, this would explain three simultaneous observations in this stage[43,45,46] : (1) gaseous CO_2 molecules would exfoliate crystal planes, (2) the oxygen content would drop and (3) forming a CO_2 molecule requires that two oxygen atoms will remove one carbon atom from the basal graphitic plane leaving a vacancy

behind, thus explaining the irreversible damage to the hexagonal graphene lattice evident in Figure 4.

Raman spectra of the GO samples oxidized for 120 min and 5 weeks do not show much change (Figure S5). In contrast to XRD and XPS observations, which provide evidence of a significant change in chemical composition as well as crystal order, there are only subtle changes in the Raman. The intensity of the D and 2D peaks slightly increased but the I_D/I_G intensity ratio remains essentially unchanged. This means that despite the stacking order and the chemical composition in GO as probed by XRD and XPS markedly evolves, the local order (defect density) examined by Raman spectroscopy is established already at 120 min and does not much change later. It also means that a chemical composition of GO doesn't play a decisive role in shaping the Raman response. Rather, a hybridization of defect sites is responsible for the intensity and line width of the Raman bands[47,48,49,50].
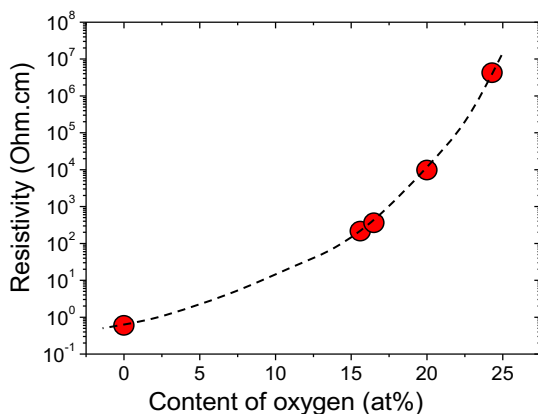

Figure 6. Dependence of the resistivity of the GO samples on the content of oxygen on a semi-logarithmic scale.

Finally, we demonstrate the effect of oxidation on a macroscopic material property, the electrical resistivity. This was measured from freestanding membranes prepared by filtration of suspended graphitic particles in water after different stages of oxidation. Figure 6 shows the

dependence of the electrical resistivity on the content of oxygen on a semi-logarithmic scale. At 25 at.% of oxygen the value of electrical resistivity has increased by seven orders of magnitude; in the sample with 31 at.% of oxygen, the resistance reaches a value beyond our instrument range.

CONCLUSIONS

The presented results indicate two phases of oxidation: the first-phase oxygen uptake of about 20 at.% was found predominantly in a form of C-O-C groups, while in other parts the graphitic spacing persists; in the second phase, the oxygen uptake above 30 at.% is mostly in a form of C=O and O-C=O groups that completely intercalate graphite. After four days of oxidation, the structure of intercalated graphite becomes unstable and spontaneously exfoliates into individual GO sheets. Two weeks of oxidation causes a significant decrease in oxygen concentration from 30 at.% down to 20 at.%. We interpret this observation to be due to spontaneous release of CO_2 causing additional structural damage and agglomeration of the exfoliated GO sheets. Our study also points out to importance of choosing proper experimental methods to characterize the products of graphite oxidation. As clearly shown, Raman spectroscopy becomes insensitive even at the early oxidation stages to structural and chemical changes in GO which, on the other hand, can be consistently traced by the XPS, XRD and electrical resistivity measurements.

ASSOCIATED CONTENT

Supporting Information.

The following files are available free of charge.

SI_skakalova (PDF)

AUTHOR INFORMATION

Corresponding Author

Dr. Viera Skakalova

E-mail: viera.skakalova@univie.ac.at

REFERENCES

(1) Eigler, S.; Dimiev, A.M. (Eds.). *Graphene Oxide: Fundamentals and Applications*; John Wiley & Sons, Inc.: Chichester, West Sussex, U.K., 2017, p. 175-229.

(2) Eigler, S.; Hirsch, A. Chemistry with Graphene and Graphene Oxide - Challenges for Synthetic Chemists. *Angewandte Chemie* **2014**, *53*, 7720–7738.

(3) Kumar, N.A.; Choi, H.J.; Shin, Y.R.; Chang, D.W.; Dai, L.; Baek, J.B. Polyaniline-Grafted Reduced Graphene Oxide for Efficient Electrochemical Supercapacitors. *ACS Nano* **2012**, *6*, 1715-1723.

(4) Zhang, L.L.; Zhao, X.; Stoller, M.D.; Zhu, Y.; Ji, H.; Murali, S.; Wu, Y.; Perales, S.; Clevenger, B.; Ruoff, R.S. Highly Conductive and Porous Activated Reduced Graphene Oxide Films for High-Power Supercapacitors. *Nano Lett*. **2012**, *12*, 1806-1812.

(5) Xing, L.B.; Hou, S.F.; Zhou, J.; Li, S.; Zhu, T.; Li Z.; Si W.; Zhuo S. UV-Assisted Photoreduction of Graphene Oxide into Hydrogels: High-Rate Capacitive Performance in Supercapacitor, *J. Phys. Chem. C* **2014**, *118*, 25924-25930.

(6) Jo, K.; Gu, M.; Kim, B.S. Ultrathin Supercapacitor Electrode Based on Reduced Graphene Oxide Nanosheets Assembled with Photo-Cross-Linkable Polymer: Conversion of Electrochemical Kinetics in Ultrathin Films. *Chem. Mater*. **2015**, *27*, 7982-7989.

(7) Li, S.S.; Tu, K.H.; Lin, C.C.; Chen C.W.; Chhowalla, M. Solution-Processable Graphene Oxide as an Efficient Hole Transport Layer in Polymer Solar Cells. *ACS Nano* **2010**, *4*, 3169-3174.

(8) Kavan, L.; Yum, J.H.; Graetzel, M. Optically Transparent Cathode for Co(III/II) Mediated Dye-Sensitized Solar Cells Based on Graphene Oxide. *ACS Appl. Mater. Interfaces* **2012**, *4*, 6999-7006.

(9) Yang, B.; Zuo, X.; Chen, P.; Zhou, L.; Yang, X.; Zhang, H.; Li, G.; Wu, M.; Ma, Y.; Jin, S.; Chen, X. Nanocomposite of Tin Sulfide Nanoparticles with Reduced Graphene Oxide in High-Efficiency Dye-Sensitized Solar Cells. *ACS Appl. Mater. Interfaces* **2015**, *7*, 137-143.

(10) Wang, Z.; Eigler, S.; Ishii,Y.; Hu,Y.; Papp, C.; Lytken,O.; Steinru, H.P.; Halik, M. A Facile Approach to Synthesize an Oxo-Functionalized Graphene/Polymer Composite for Low-Voltage Operating Memory Devices, *J. Mater. Chem. C* **2015**, *3*, 8595-8604.

(11) Weaver, C.L.; LaRosa, J.M.; Luo, X.; Cui, X.T. Electrically Controlled Drug Delivery from Graphene Oxide Nanocomposite Films. *ACS Nano* **2014**, *8*, 1834-1843.

(12) He, X.P.; Deng, Q.; Cai, L.; Wan,g C.Z.; Zang, Y.; Li, J.; Chen, G.R.;Tian, H. Fluorogenic Resveratrol-Confined Graphene Oxide For Economic and Rapid Detection Of Alzheimer's Disease. *ACS Appl. Mater. Interfaces* **2014**, *6*, 5379-5382.

(13) Song, J.; Yang, X.; Jacobson, O.; Lin, L.; Huang, P.; Niu, G.; Ma, Q; Chen, X. Sequential Drug Release and Enhanced Photothermal and Photoacoustic Effect of Hybrid Reduced Graphene Oxide-Loaded Ultrasmall Gold Nanorod Vesicles for Cancer Therapy. *ACS Nano* **2015**, *9*, 9199-9209.

(14) Ocsoy, I.; Paret, M.L.; Ocsoy, M.A.; Kunwar, S.; Chen, T.; You, M.; Tan, W. Nanotechnology in Plant Disease Management: DNA-Directed Silver Nanoparticles on Graphene Oxide as an Antibacterial against Xanthomonas perforans. *ACS Nano* **2013**, *7*, 8972-8980.

(15) Kromka, A.; Jira, J.; Stenclova, P.; Kriha, V.; Kozak, H.; Beranova, B.; Vretenar, V.; Skakalova, V.; Rezek, B. Bacterial Response to Nanodiamonds and Graphene Oxide Sheets, *Phys. Status Solidi B* **2016**, *253*, 2481–2485

(16) Brodie; B.C. *Philos. Trans. R. Soc. London* **1859**, *149*, 249-259.

(17) Staudenmaier, L. *Ber. Dtsch. Chem. Ges.* **1898**, *31*, 1481-1487.

(18) Hummers, W.S.; Offeman, R.E. *J. Am.Chem. Soc.* **1958**, *80*, 1339-1339.

(19) Yalcin, S.E.; Galande, C.; Kappera, R.; Yamaguchi, H.; Martinez, U.; Velizhanin, K.A.; Doorn, S.K.; Dattelbaum, A.M.; Chhowalla, M.; Ajayan, P.M.; Gupta G.; Mohite, A.D. Direct Imaging of Charge Transport in Progressively Reduced Graphene Oxide Using Electrostatic Force Microscopy. *ACS Nano* **2015**, *9*, 2981-2988.

(20) Muchharla, B.; Narayanan, T.N.; Balakrishnan, K.; Ajayan, P.M.; Talapatra, S. Temperature Dependent Electrical resistivity of Disordered Reduced Graphene Oxide. *2D Mater.* **2014**, *1*, 011008.

(21) Wang, S.W.; Lin, H.E.; Lin, H.D.; Chen, K.Y.; Tu, K.H.; Chen, C.W.; Chen, J.Y.; Liu, C.H.; Liang, C.T.; Chen, Y.F. Transport Behavior and Negative Magnetoresistance in Chemically Reduced Graphene oxide Nanofilms, *Nanotechnology* **2011**, *22*, 335701.

(22) Vianelli, A.; Candini, A.; Treossi, E.; Palermo, V.; Affronte, M. Observation of Different Charge Transport Regimes and Large Magnetoresistance in Graphene Oxide Layers. *Carbon* **2015**, *89*, 188 –196.

(23) Gómez-Navarro, C.; Weitz, R.T.; Bittner, A.M.; Scolari, M.; Mews, A.; Burghard, M.; Kern, K. Electronic Transport Properties of Individual Chemically Reduced Graphene Oxide Sheets, *Nano Letters* **2007**, *7*, 3499-3503.

(24) Chang-Jian, S.K.; Ho, J.R.; Cheng, J.W.J.; Hsieh, Y.P. Characterizations of Photoconductivity of Graphene Oxide Thin Films, *AIP Advances* **2012**, *2*, 022104.

(25) Kaiser, A.B.; Gómez-Navarro, C.; Sundaram, R.S.; Burghard, M.; Kern, K.. Electrical Conduction Mechanism in Chemically Derived Graphene Monolayers, *Nano Letters* **2009**, *9*, 1787-1792.

(26) Pei, S.; Zhao, J.; Du, J.; Ren, W.; Cheng, H.M. Direct Reduction of Graphene Oxide Films into Highly Conductive and Flexible Graphene Films by Hydrohalic Acids. *Carbon* **2010**, *48*, 4466-4474.

(27) Dimiev, A.; Kosynkin, D.V.; Alemany, L.B.; Chaguine, P.; Tour, J.M. Pristine Graphite Oxide. *J. Am. Chem.Soc.* **2012**, *134*, 2815-2822.

(28) Dimiev, A.M.; Tour, J.M. Mechanism of Graphene Oxide Formation. *ACS Nano* **2014**, *8*, 3060-3068.

(29) Shao, G.; Lu, Y.; Wu, F.; Yang, Ch.; Zeng, F.; Wu, Q. Graphene Oxide: the Mechanisms of Oxidation and Exfoliation. *J Mater Sci* **2012**, *47*, 4400-4409.

(30) Gómez-Navarro, C.; Meyer, J.C.; Sundaram, R.S.; Chuvilin, A.; Kurasch, S.; Burghard, M.; Kern, K.; Kaiser, U. Atomic Structure of Reduced Graphene Oxide, *Nano Lett.* **2010**, *10*, 1144–1148.

(31) Krishnamoorthy, K.; Veerapandian, M.; Yun, K.; Kim, S.J. The Chemical and Structural Analysis of Graphene Oxide with Different Degrees of Oxidation. *Carbon* **2013**, *53*, 38-49.

(32) Storm, M.M.; Overgaard, M.; Younesi, R.; Abildgaard Reeler, N.E.; Vosch, T.; Nielsen, U.G.; Edström, K.; Norby, P. Reduced Graphene Oxide for Li-Air Batteries: the Effect of Oxidation Time and Reduction Conditions for Graphene Oxide. *Carbon* **2015**, *85*, 233-244.

(33) Pham, T.A.; Kim, J.S.; Kim, J.S.; Jeong, Y.T. One-Step Reduction of Graphene Oxide with L-Glutathione. *Colloids and Surfaces A: Physicochem. Eng. Aspects* **2011**, *384*, 543-548.

(34) Cooper, V.R. Van der Waals Density Functional: An Appropriate Exchange Functional. *Phys. Rev. B* **2010**, *81***,** 161104.

(35) Enkovaara, J.; Rostgaard, C.; Mortensen, J.J.; Chen, J.; Dułak, M.; Ferrighi, L.; Gavnholt, J.; Glinsvad, C.; Haikola, V.; Hansen, H.A.; et al. Electronic Structure Calculations with GPAW: A Real-Space Implementation of the Projector Augmented-Wave Method. *J. Phys.: Condens. Matter* **2010**, *22***,** 253202.

(36) Wu, Z.S.; Winter, A.; Chen, L.; Sun, Y.; Turchanin, A.; Feng, X.; Müllen, K. Three-Dimensional Nitrogen and Boron Co-doped Graphene for High-Performance All-Solid-State Supercapacitors. *Adv. Mater.* **2012**, *24*, 5130–5135.

(37) Wu, Z.S.; Winter, A.; Chen, L.; Sun, Y.; Turchanin, A.; Feng, X.; Müllen, K. Three-Dimensional Nitrogen and Boron Co-doped Graphene for High-Performance All-Solid-State Supercapacitors. *Adv. Mater.* **2012**, *24*, 5130–5135.

(38) Dimiev, A.M.; Ceriotti, G.; Behabtu, N.; Zakhidov, D.; Pasquali, M.; Saito, R.; Tour, J.M. Direct Real-Time Monitoring of Stage Transitions in Graphite Intercalation Compounds. *ACS Nano* **2013**, *7*, 2773-2778.

(39) Shao, G.; Lu, Y.; Yang, Ch.; Zeng, F.; Wu, Q. Graphene Oxide: the mechanisms of oxidation and exfoliation. *J. Mater. Sci.* **2012**, *47*, 4400-4409.

(40) Diez-Betriu, X.; Alvarez-Garcia, S.; Botas, C.; Alvarez, P.; Sanchez-Marcos, J.; Prieto, C.; Menendez, R.; de Andres, A. *J. Mater. Chem. C* **2013**, *1*, 6905-6912.

(41) Haubner, K.; Murawski, J.; Olk, P.; Eng, L.M.; Ziegler, Ch.; Adolphi, B.; Jaehne, E. The Route to Functional Graphene Oxide. *ChemPhysChem* **2010**, *11*, 2131 – 2139.

(42) Cancado, L.G.; Jorio, A.; Martins Ferreira, E.H.; Stavale, F.; Achete, C.A.; Capas, R.B.; Moutinho, M.V.O.; Lombardo, A.; Kulmala, T.S.; Ferrari, A.C. Quantifying Defects in Graphene via Raman Spectroscopy at Different Excitation Energies, *Nano Letters* **2011**, *11*, 3190-3196.

(43) Englert, J.M.; Vecera, P.; Knirsch, K.C.; Schäfer, R.A.; Hauke, F.; Hirsch, A. Scanning Raman Microscopy for the Statistical Analysis of Covalently Functionalized Graphene. *ACS Nano* **2013**, *7*, 5472-5482.

(44) Lee, D.W.; Seo, J.W.. sp^2/sp^3 Carbon Ratio in Graphite Oxide with Different Preparation Times. *J. Phys. Chem. C* **2011**, *115*, 2705-2708.

(45) Eigler, S.; Grimm, S.; Enzelberger-Heim, M.; Müller, P.; Hirsch, A. Graphene Oxide: Efficiency of Reducing Agents. *Chem. Commun.* **2013**, *49*, 7391-7393.

(46) Dreyer, D.R.; Park, S.; Bielawski, C.W.; Ruoff, R.S. The Chemistry of Graphene Oxide. *Chem. Soc. Rev.* **2010**, *39*, 228-240.

(47) Yang, S.; Zhi, L.; Tang, K.; Feng, X.; Maier, J.; Müllen, K. Efficient Synthesis of Heteroatom (N or S)-Doped Graphene Based on Ultrathin Graphene Oxide-Porous Silica Sheets for Oxygen Reduction Reactions. *Adv. Funct. Mater.* **2012***, 22,* 3634–3640.

(48) Rümmeli, M.H.; Zeng, M.; Melkhanova, S.; Gorantla, S.; Bachmatiuk, A.; Fu, L.; Yan, Ch.; Oswald, S.; Mendes, R.G.; Makarov, D.; Schmidt, O.; Eckert, J. Insights into the Early Growth of Homogeneous Single-Layer Graphene over Ni–Mo Binary Substrates. Chem. Mater. **2013***, 25,* 3880–3887.

(49) Pang, J.; Bachmatiuk, A.; Fu, L.; Mendes, R.G.; Libera, M.; Placha, D.; Martynková, G.S.; Trzebicka, B.; Gemming, T.; Eckert, J.; Rümmeli, M.H. Direct synthesis of graphene from adsorbed organic solvent molecules over copper. *RSC Adv.* **2015**, *5*, 60884-60891

(50) Pang, J.; Bachmatiuk, A.; Ibrahim, I.; Fu, L.; Placha, D.; Martynkova, G.S.; Trzebicka, B.; Gemming, T.; Eckert, J.; Rümmeli, M.H. CVD growth of 1D and 2D sp2 carbon nanomaterials. *J Mater Sci.* **2016**, *51*, 640
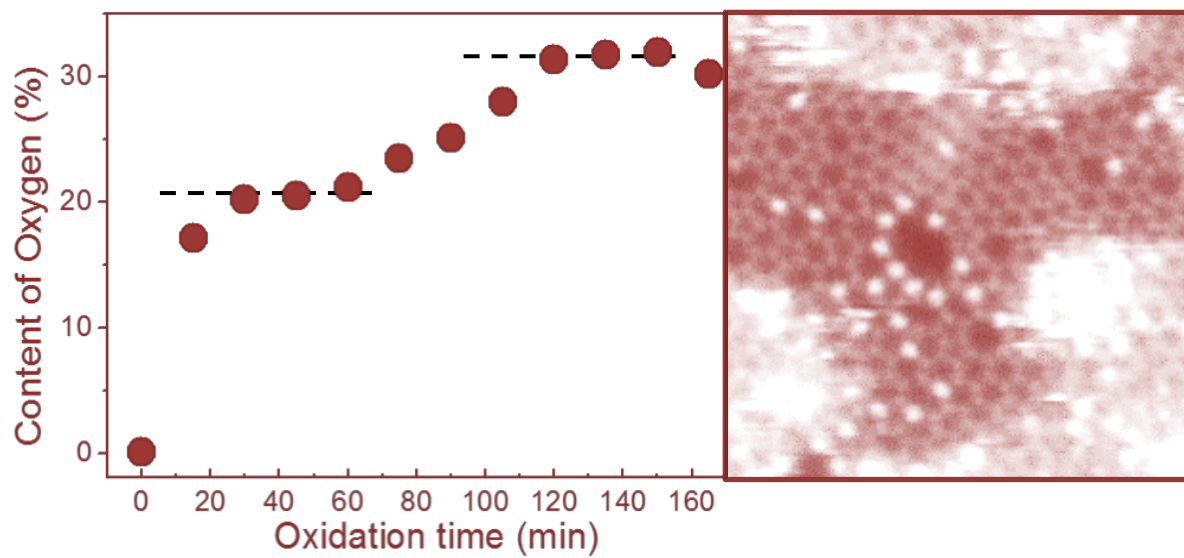
SUPPORTING INFORMATION

Chemical oxidation of graphite: evolution of the structure and properties

Viera Skákalová[1,2,], Peter Kotrusz[1], Matej Jergel[4], Toma Susi[2], Andreas Mittelberger[2], Viliam Vretenár[1,5], Peter Šiffalovič[4], Jani Kotakoski[2], Jannik C. Meyer[2] and Martin Hulman[1,3]*

[1]Danubia NanoTech, Ilkovičova 3, 84104 Bratislava, Slovakia

[2]University of Vienna, Boltzmanngasse 5, 1090 Vienna, Austria

[3]Institute of Electrical Engineering SAS, Dúbravská cesta 9, 84104 Bratislava, Slovakia

[4]Institute of Physics SAS, Dúbravská cesta 9, 84104 Bratislava, Slovakia

[5]Center for Nanodiagnostics of SUT, Vazovova 5, 81000 Bratislava, Slovakia

*Corresponding author. E-mail: viera.skakalova@univie.ac.at (Viera Skákalová)

Electrical resistivity measurement of the filtrated graphite oxide samples was described in the main article Experimental Section. Figure S1 shows the sample holder consisting of a system of 20 pins, where a Si/SiO_2 chip fixed in the center square serves as a substrate for our GO layer. 4-probe configuration is realized by four parallel gold stripes evaporated on the sample to applying current between the outer stripes and sensing potential drop between the two central stripes. Values of the electrical resistivity were determined from current-voltage characteristics measured at room temperature and plotted in main article Fig. 6.
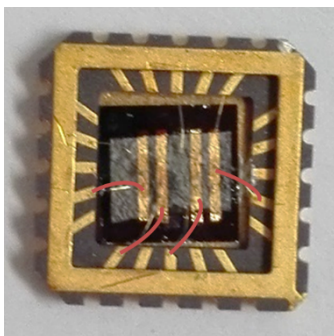

Figure S1 4-probe configuration setup used for the electrical resistivity measurement of oxidized graphite.

The observed variations of carbon bonding states as a consequence of increasing concentration of strong oxidizing agent during graphite oxide synthesis (Experimental Section) are summarized in Table S1. The quantitative evaluation is based on peak fitting of XPS spectra of fractions taken at different stages of the synthesis. The sp^2 C-C bonding state progressively changes to C-O-C first and to O-C=O later. A dramatic chance is observed to the end of the process when ~37% of C-O-C apparently transforms to C=O accompanied with C sp^3 hybridization.

Table S1 Content of carbon bonding states in the course of the oxidative intercalation process

Processing time (min)	Portion of OA (%)	C-C sp^2 284.5 eV (%)	C sp^3 285.6 eV (%)	C-O-C 286.6 eV (%)	C=O 287.5 eV (%)	O-C=O 288.6 eV (%)
0	0	100,0	0,0	0,0	0,0	0,0
30	20	86,9	0,0	13,1	0,0	0,0
75	50	69,7	0,0	18,8	0,0	11,5
105	70	54,2	0,0	37,1	0,0	8,7
120	80	0,0	37,3	0,0	36,0	26,7

In addition to the extensive characterization of oxidation of graphitic grains smaller than 20 μm, we investigated how a size of the source graphitic grains affects the interlayer distance after oxidation (Figure S1A). A shift of the XRD peak position to larger angles (a reduction in interlayer distance d) is observed when a larger average size of the source graphitic grain is used for oxidation; the grains smaller than 20 μm result in $d = 0.820$ nm whereas those of the size up to 150 μm lead to $d = 0.804$ nm after oxidation.
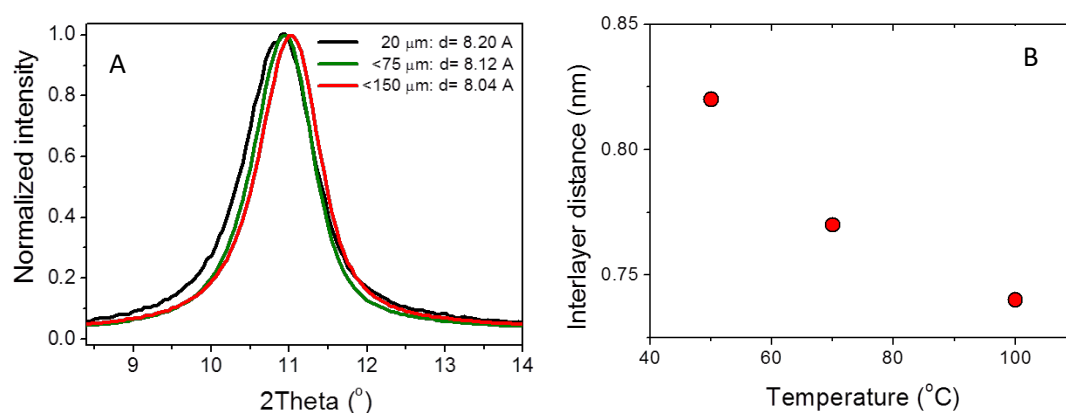

Figure S2 Comparison of interlayer distance determined by XRD (A) for different grain sizes of starting graphitic powder, (B) after drying the GO dispersion at temperatures of 50, 70 and 100 ºC.

Another aspect influencing the interlayer distance of the graphite oxide is the temperature used for drying the suspensions of GO. Figure S2B demonstrates a significant reduction in the interlayer distance of graphite oxide with increasing temperature of drying: $d = 0.820$ nm found after drying at 50 °C drops to only $d = 0.735$ nm when dried at 100 °C.

Figure S3 represents the STEM/EELS measurement of GO deposited on a TEM grid. Besides carbon, the spectrum identifies silicon and oxygen in the sample in significant concentrations.
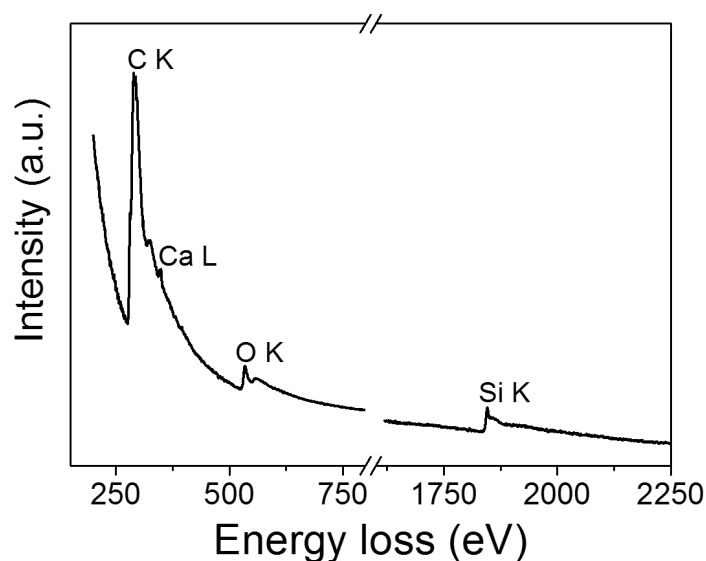

Figure S3 EELS spectrum of GO deposited on a TEM grid measured inside the STEM

Figure S4 (left) presents an AFM image of exfoliated GO flakes prepared by our oxidation process. On the right of the AFM image there are two height profiles along the lines 1 and 2 marked on the AFM image. A typical height for a single layer of GO measured on a Si substrate is about 1 nm; in the both height profiles the smallest steps of 1 nm correspond to the thinnest parts of the GO flakes, whereas multiples of this height are measured in the folded parts of the flakes. The color render indicates the majority of the displayed GO flakes are exfoliated into single layers.
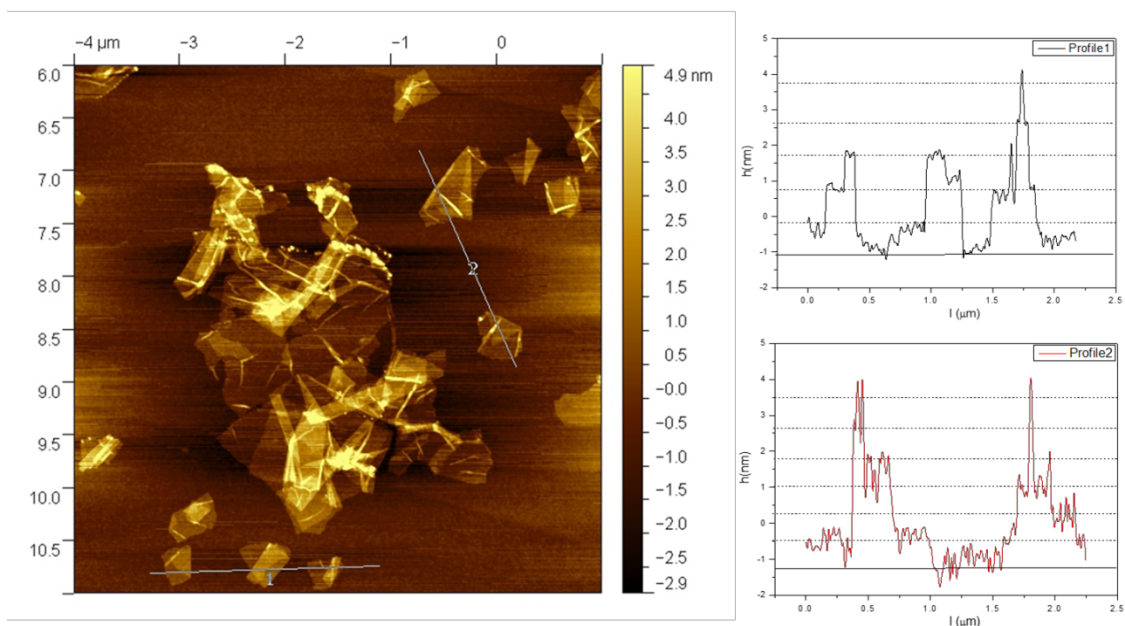
Figure S4 (left) AFM image of exfoliated GO prepared by our oxidation process; (right) height profiles along the lines 1 and 2 of the AFM image.

Raman spectra in Fig. S5 compare the sample oxidized for 120 min to that treated for 5 weeks. The intensity of the D and 2D peaks slightly increased but the I_D/I_G intensity ratio remains essentially unchanged, showing that the local order (defect density) examined by Raman spectroscopy is established already at 120 min and does not much change later.
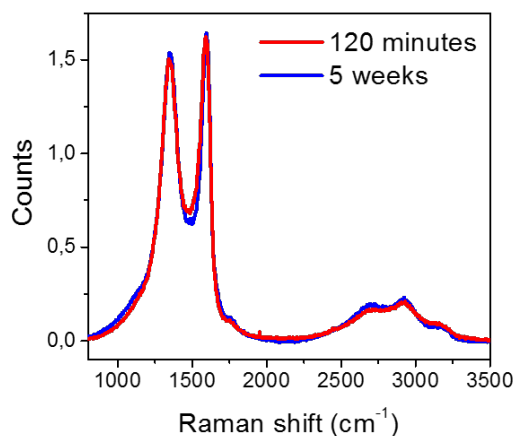

Figure S5 Comparison of Raman spectra of GO oxidized for 120 min (red) and 5 weeks (blue).